Rev.Adv.Mater.Sci. 23(2010) 196-206

ELECTRON PARAMAGNETIC RESONANCE STUDY OF MAGNETIC CENTERS IN $FeSbVO_6$

J. Typek[1], N. Guskos[1,2], E. Filipek[3] and M. Piz[3]

[1]Institute of Physics, West Pomeranian University of Technology, Al. Piastow 48, 70-311 Szczecin, Poland
[2]Solid State Physics, Department of Physics, University of Athens, Panepistimiopolis, 15 784 Zografos, Athens, Greece
[3]Department of Inorganic and Analytical Chemistry, West Pomeranian University of Technology, Al. Piastow 17, 70-310 Szczecin, Poland

Received: December 10, 2009

Abstract. $FeSbVO_6$ powder samples synthesized by the solid state reaction technique were investigated by the Electron Paramagnetic Resonance (EPR) in the 4-300K temperature range. At room temperature the EPR spectrum consists of two components: a narrow line centered at g = 1.975 and a more intense and much broader Lorentzian line centered at g = 2.20. The broad line was deconvoluted on three spectral Lorentzian components to properly reproduce the temperature dependence of the observed EPR spectra. The temperature dependence of the EPR spectral parameters (linewidth, g-factor, amplitude, integrated intensity) of all components was calculated. At low temperature (T < 100K) the main component of the broad line displayed very interesting behavior by reaching a maximum in the integrated intensity at 70K. The narrow line in the EPR spectrum of $FeSbVO_6$ was attributed to strongly interacting V^{4+} monomers, while the broad line was produced by various iron and vanadium spin clusters. A comparison of the magnetic properties of $FeSbVO_6$ with the previously studied $CrSbVO_6$ was done and the observed differences are discussed. Possible models of the discovered paramagnetic centers were proposed.

1. INTRODUCTION

Recent years have brought increased interest in catalysts containing vanadium, especially those in which vanadium plays a role of an active phase [1-13]. Among various investigated new catalysts of oxidation reactions of light hydrocarbons the most promising catalysts for technological applications appear to be those involving V_2O_5, α-Sb_2O_4 and Fe_2O_3 or Cr_2O_3 as well as compounds synthesized from these oxides [1,4-15]. The study of the physicochemical properties of phases formed in a system containing catalysts could provide a very useful knowledge about the solid's surface on which elementary catalytic reactions take place. Our studies on the ternary oxide system V_2O_5-Cr_2O_3-a-Sb_2O_4, have shown that the system components interact in the solid state producing a compound with the formula $CrSbVO_6$ [16]. The structure, thermal and magnetic properties of $CrSbVO_6$ have been investigated [16-18]. The literature data indicate that catalysts containing $CrSbVO_6$ are active in the reaction of obtaining acrylonitrile by ammooxidation of propane [4-5]. A literature survey has shown that an analogue system, *i.e.,* V_2O_5-Fe_2O_3-α-Sb_2O_4 and the reactions taking place therein have not been studied comprehensively [19]. The obtained results have shown that a new compound, $FeSbVO_6$, is formed in this system. This compound could be obtained both from V_2O_5, α-Sb_2O_4 and Fe_2O_3 oxides, and from the mixture of $FeVO_4$ and α-Sb_2O_4 at a molar ratio

Corresponding author: J. Typek, e-mail: typian@zut.edu.pl

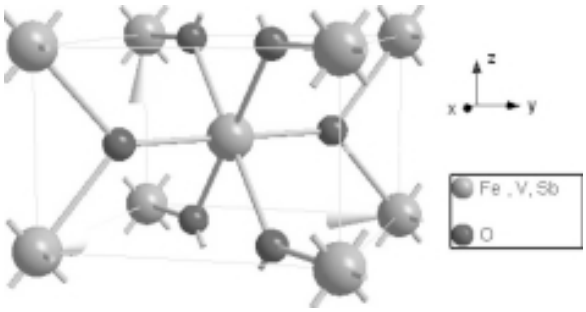

Fig. 1. Unit cell of rutile-type $FeSbVO_6$. Metal ions (Fe, V, Sb) are placed in octahedral positions.

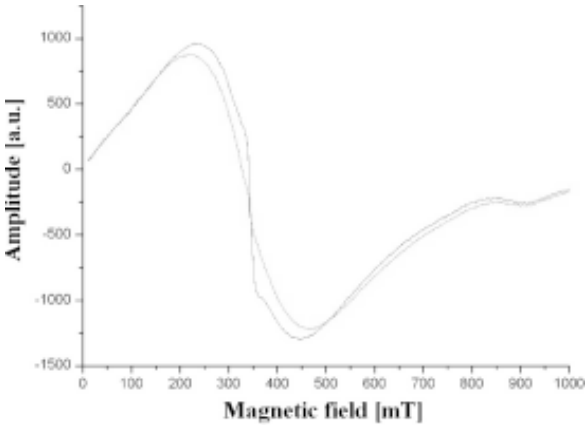

Fig. 2. Room temperature EPR spectra of $FeSbVO_6$ synthesized in argon (black line) and in air atmosphere (red line).

of 2:1.The synthesis could be carried out in argon or in air atmosphere. The compound is stable in air up to ~1260K [19]. The $FeSbVO_6$ compound crystallizes in a rutile-type structure (space group $P4_2/mnm$, $Z = 2$). The unit cell has a tetragonal symmetry and the structure is built from deformed CrO_6, VO_6, and SbO_6 octahedra (Fig. 1). Each octahedron shares one edge with the adjacent members of the chain. Alternatively, the crystal structure may be visualized as chains of ions -O-M-O-O-M-O-, where M = Cr, V, Sb. All chains in the same layer are parallel, and the chains in adjacent layers are perpendicular to one another and to the *c*-axis. In the real structure the oxygen deficiency is expected which involves the change of oxidation states of metal ions. The question of oxidation states of metal ions in non-stoichiometric rutile-type compounds has been the subject of some controversy and is of great importance for the interpretation of catalytic mechanisms.

The aim of this work is to investigate, using the electron paramagnetic resonance (EPR) method, magnetic properties of $FeSbVO_6$ synthesized from V_2O_5, Fe_2O_3, and α-Sb_2O_4 oxides. Up to now no data about magnetic properties of $FeSbVO_6$ have been published. The EPR spectra, registered in a wide temperature range will be analyzed and a comprehensive picture of magnetic interactions will be deduced from the temperature dependence of the EPR spectral parameters (*g*-factor, linewidth, integrated intensity).

2. EXPERIMENTAL

The following oxides were used for the synthesis of $FeVSbO_6$: analytically pure (a.p.) Fe_2O_3 (POCH, Gliwice, Poland), a.p. V_2O_5 (POCH, Gliwice, Poland), a.p. Sb_2O_3 (Merck, Germany) and α-Sb_2O_4 obtained by calcinations of Sb_2O_3 in air [20]. Pure $FeSbVO_6$ was prepared by heating pressed equimolar mixtures of Fe_2O_3, V_2O_5, and Sb_2O_3 or a Sb_2O_4 powdered oxides in air or argon atmosphere using the procedure given in work [19]. $FeSbVO_6$ was synthesized according to the equations:

$$Fe_2O_{3(s)} + Sb_2O_{3(s)} + V_2O_{5(s)} + 1/2\,O_{2(g)} = 2\,FeSbVO_{6(s)} \ (\text{in air}),$$

$$Fe_2O_{3(s)} + a\text{-}Sb_2O_{4(s)} + V_2O_{5(s)} = 2\,FeSbVO_{6(s)} \ (\text{in argon}).$$

Having been weighed in suitable proportions, the oxides were homogenized and calcinated at temperatures up to 1073K in 24 h stages. When the diffraction patterns taken after two consequent heating cycles were identical to the pattern of $FeSbVO_6$ both with respect to the positions and the intensities of the recorded diffraction lines, it was assumed that the samples were monophases. The phase composition of the samples was determined by an X-ray phase analysis with the aid of a DRON-3 diffractometer (Bourevestnik, Sankt Petersburg, Russia) using the CoK_α/Fe radiation. The diffraction patterns of monophase sample corresponded to that calculated from the literature data [19].

The EPR measurements were performed on a conventional X-band (ν = 9.4 GHz) Bruker E 500 spectrometer with 100 kHz magnetic field modulation. Samples containing around 20 mg of $FeSbVO_6$ powder were placed in 4 mm diameter quartz tubes. The measurements were carried out in the temperature range from RT down to the liquid helium tem-

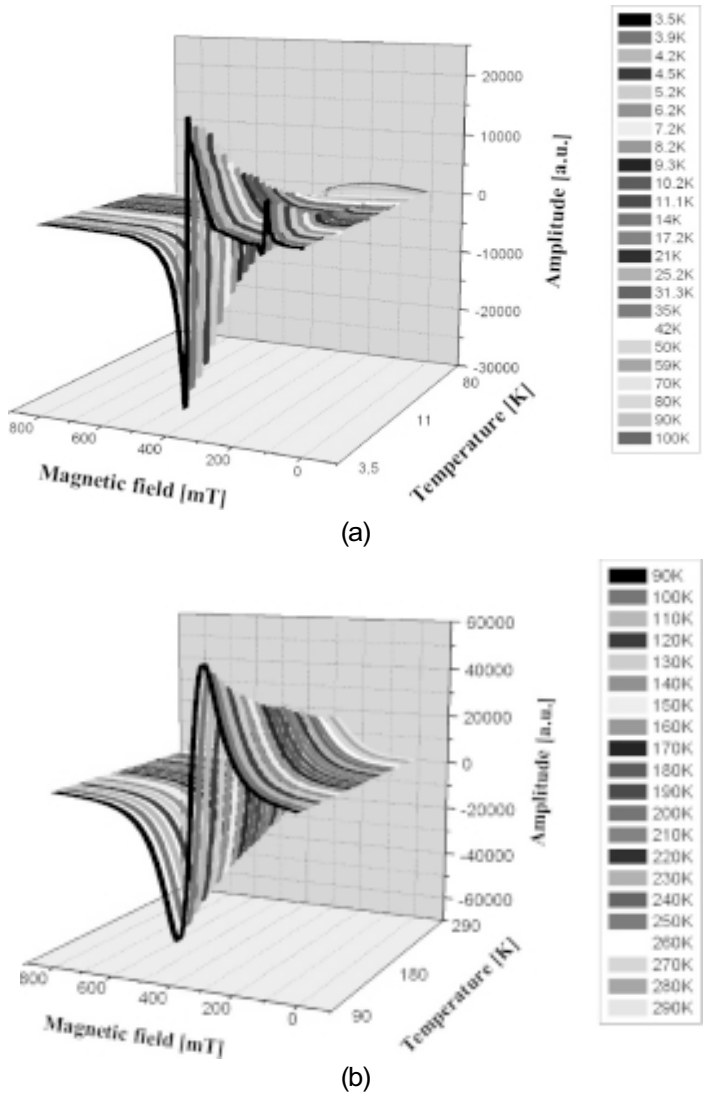

Fig. 3. EPR spectra of $FeSbVO_6$ at different temperatures: (a) low temperature range 3.5-100K; (b) high temperature range 90-290K.

perature with the $\Delta T = \pm 1.0$K stability using the Oxford cryogenic system.

3. RESULTS AND DISCUSSION

As two types of $FeSbVO_6$ samples were produced, one synthesized in an argon atmosphere and the other in air, an attempt was made to detect differences in their EPR spectra. It should be mentioned that the registered XRD patterns were exactly the same for both types of samples. Fig. 2 presents the EPR spectra taken at RT of two specific samples: samples synthesized in argon (black line) and in air (red line) registered at the same spectrometer conditions and normalized to a unit sample mass. The sample produced in argon generates a slightly more intense and narrower signal than the air sample but the difference is not large and it is sample dependent. It should be noticed that a reverse intensity ratio was observed for the $CrSbVO_6$ compound. A narrow line attributed to V^{4+} ions is more visible in the argon sample due to a narrower signal from Fe^{3+} ions. As both types of samples showed similar temperature behavior of their EPR spectra it is only samples synthesized in argon that will be further considered.

A standard sample of carefully weighted polycrystalline $VOSO_4 5H_2O$ was used to estimate the number of spins participating in a resonance. Measurements of the intensity of any EPR spectrum are generally quite imprecise. Although care was

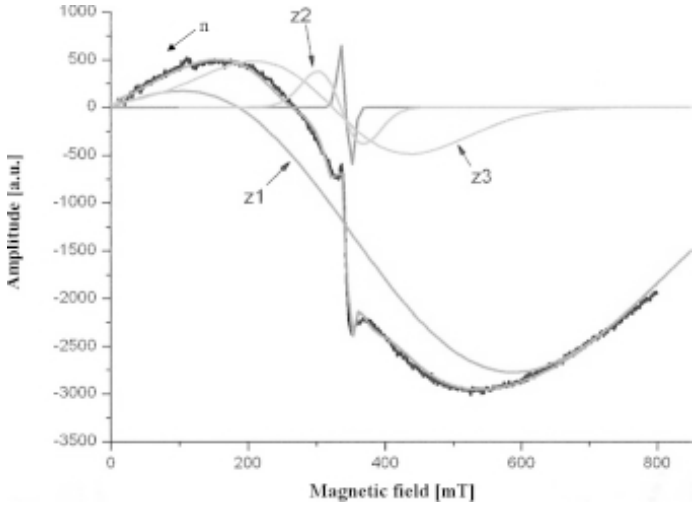

Fig. 4. Decomposition of of $FeSbVO_6$ EPR spectrum registered at 90K (solid line) on four components and the sum of these components (red line). The narrow line is designated as *n*, while the three components of the broad line are designated as *z1*, *z2*, and *z3*.

taken to maintain the same modulation and power levels, these precautions did not guarantee identical conditions in the microwave cavity since the dielectric properties of the sample and the used standard were not identical. Taking into account these circumstances and the uncertainties in determining the sample and standard mass the obtained results were accurate only to the order of magnitude. It was found that the observed EPR signal corresponded to the expected bulk concentration of Fe^{3+} and V^{4+} ions in stoichiometric $FeSbVO_6$.

A selection of the registered EPR spectra is presented in Fig. 3. The spectra taken in the 90-290K 3.8-100K ranges are shown in the upper and lower panel, respectively. At high temperatures the spectrum is predominated by a broad (~150 mT), nearly Lorentzian-shaped line. Its amplitude increases with the temperature decreasing from RT, however this trend reverses and the line weakens below 70K. At low temperatures, a narrow line (~14 mT) gains intensity as the temperature decreases. A few spectral features could be registered at a low magnetic field (80-160 mT) in the same temperature range (Fig. 3a). These lines will be designated generally as low-field lines and are discussed later. As the EPR spectrum seems to consist of several components at any temperature, the registered spectra were deconvoluted. As at least one component was very broad and its linewidth became comparable to the resonance field, the lines at negative magnetic fields were taken into consideration. The absorption at negative field was a consequence of the used linearly polarized microwave field.

In Fig. 4 the decomposition of an EPR spectrum taken at 90K is presented. A very good fitting could be achieved by using four Lorentzian lines that are designated as *n*, *z1*, *z2*, and *z3*. The line designated as *n* is narrow and although visible in the whole 4-300K range, it dominates the spectrum at low temperatures. The line *z1* is very broad and it is most intense at 70K, decreasing in intensity with the decreasing temperature. The lines *z2* and *z3*, although not as intense as line *z1*, are necessary for a proper description of the obtained EPR spectra at least for temperatures T<100K.

The temperature dependence of the EPR spectra will be analysed in terms of the following basic parameters: signal amplitude A, peak-to-peak linewidth ΔB, effective g-factor and the EPR integrated intensity. This is a standard procedure used in analysis of the temperature behaviour of an EPR spectrum [20] and the definition of the used parameters is the same as in Ref. [18].

Since the Fe^{3+} ion belongs to the d^5 configuration with the ^6S ground state there is no spin-orbit coupling. As a result, it is expected that the g-factor will be very near to the free ion g value, i.e. 2.0023. However, when certain symmetry elements are present the spin Hamiltonian is usually expressed as [21]

$$H = g\beta BS + D\left[S_z^2 - \{S(S+1)/3\}\right] + E\left(S_x^2 - S_y^2\right),$$

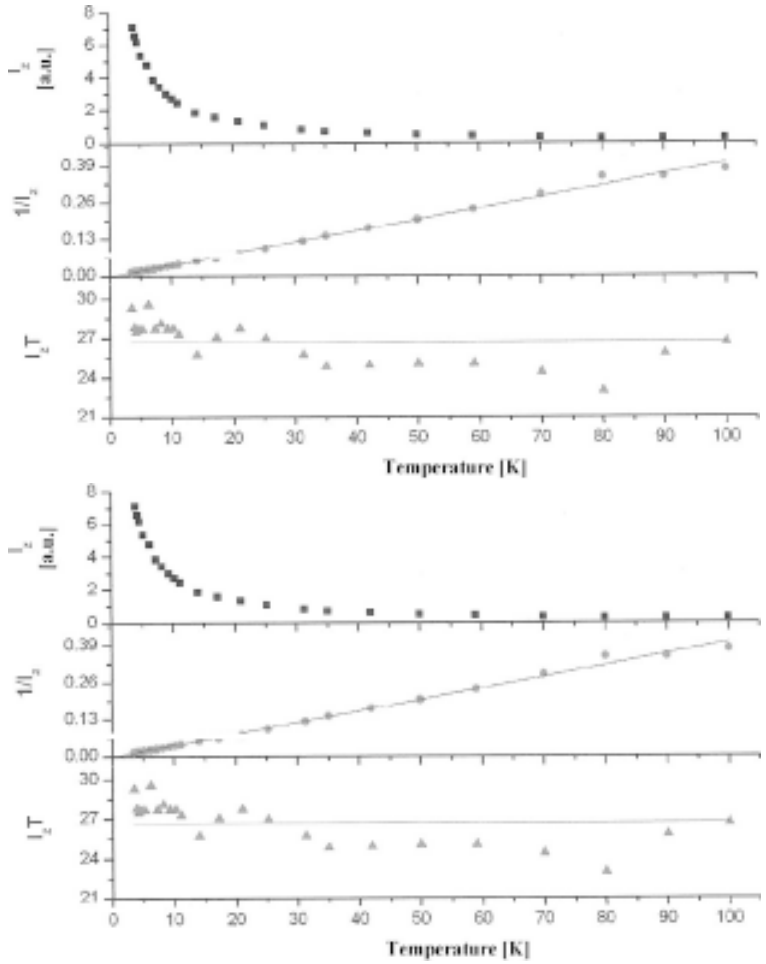

Fig. 5. Temperature dependence of EPR parameters for the narrow line: (a) amplitude, *g*-factor and linewidth; (b) integrated intensity, the reciprocal of integrated intensity and the product of integrated intensity and temperature.

where $S = 5/2$, D, and E are the axial and rhombic structure parameters. The often used parameter called rhombicity, $\lambda = E/D$, which quantifies the degree of rhombic distortion of the electronic environment is limited to $0 \le \lambda \le 1/3$. The $^6S_{5/2}$ ground state of Fe^{3+} free ion is expected to split into three Kramers doublets $|\pm 5/2>$, $|\pm 3/2>$, and $|\pm 1/2>$ with the energy separation normally greater than the microwave quantum. The *g*-values are dependent on both λ and $D/h\nu$, where hn is the energy of the microwave quantum. The parameter λ is directly related to the ion environment symmetry, $\lambda = 0$ representing axial symmetry and $\lambda = 1/3$ a completely orthorhombic case in which the three Kramers doublets are equally split by the crystal field. When $D > h\nu$, it can be predicted that for $\lambda = 0$ resonances at $g_{\|} = 2.0$ and $g_{\perp} = 6.0$ for the lowest doublet are expected. For $\lambda = 1/3$, an isotropic resonance is predicted at $g = 4.3$ for the central doublet, and extremely anisotropic lines for the upper and lower doublets [22]. For the case of pure rhombic symmetry, i.e. $E/D = 1/3$, the $g = 4.3$ resonance is isotropic and lacks structural features [23]. Fine structure features begin to appear for small deviations from rhombic symmetry toward axial symmetry (E/D~1/3). Features at lower field near $g = 6$. are produced by larger deviations in E/D from 1/3 as the ligand field symmetry becomes more axial.

Vanadium ions exhibit a wide range of stable oxidation states including often-encountered 3+, 4+, and 5+ states. In many materials the majority of vanadium exists in paramagnetic oxovanadium(IV) VO^{2+} ions which are complexed in some form. Various V^{4+} species could be detected by the EPR technique. V^{4+} clusters give rise to a broad signal owing to significant dipolar interactions, whereas isolated V^{4+} species exhibit a hyperfine structure derived from the interaction of free electrons ($3d^1$) with the mag-

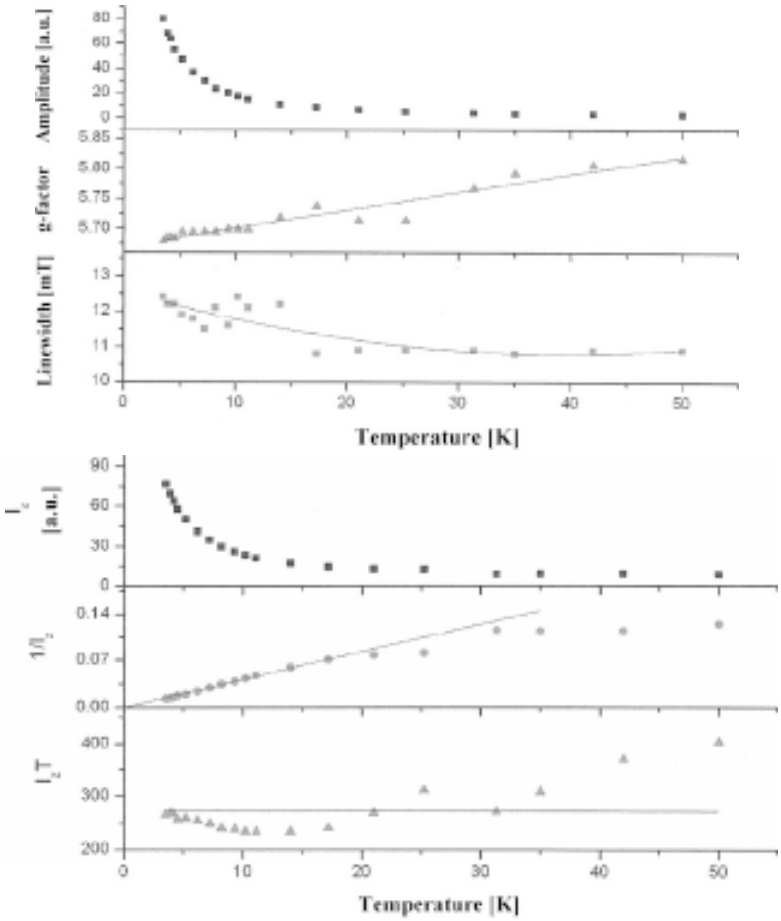

Fig. 6. Temperature dependence of EPR parameters for the low-field line: (a) amplitude, *g*-factor and linewidth; (b) integrated intensity, the reciprocal of integrated intensity and the product of integrated intensity and temperature.

netic nuclear moment of ^{51}V (I = 7/2). In this case, the EPR signal splits eightfold. In solids, the hyperfine structure can be substantially suppressed or even disappear due to various interactions of electron spins with their surroundings. For example, in conducting vanadate glasses (V_2O_5–TeO_2) such interaction occurs via the so-called super-exchange of electrons, i.e. the hopping of a mobile electron along V^{4+}–O–V^{5+} bonds [24].

Fig. 5 presents the temperature dependence of the EPR parameters for a narrow line observed in the magnetic resonance spectra of $FeSbVO_6$. This line is visible in the whole investigated temperature range, but at high temperatures it competes with an intense and broad line and it is difficult to perceive it. Its amplitude increases with the decreasing temperature and this trend is particularly strong below 20K. The *g*-factor of this line does not change with temperature and is equal to 1.9755. Its linewidth increases rather slowly with a temperature decrease. All this clearly indicates that this line should be attributed to strongly coupled V^{4+} ions or VO^{2+} complexes. The expected hyperfine lines must be suppressed by these strong interacting paramagnetic species. The temperature dependence of the integrated intensity (Fig. 5b) follows the Curie-Weiss law with the Curie-Weiss constant Θ_{CW} =3K indicating a ferromagnetic interaction of magnetic species. This is reflected in a relatively low increase in the effective magnetic moment with the decreasing temperature (Fig. 5b, lower panel).

Fig. 6 shows the temperature dependence of EPR parameters for the low-field line. This line is clearly discernable only at low temperatures. The amplitude of this line increases strongly, its *g*-factor decreases and the linewidth increases with a temperature decrease (Fig. 6a). This low-field line actually consists of at least two components and many accompanying weak lines. All these lines are most probably attributed to the Fe^{3+} ions located at

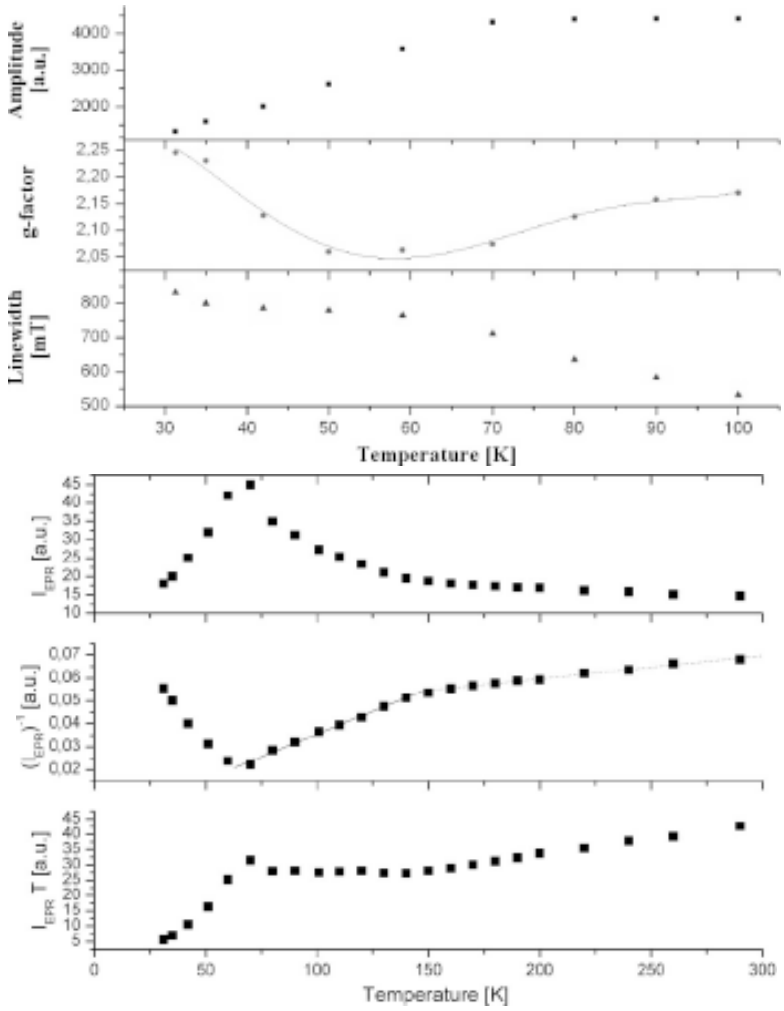

Fig. 7. Temperature dependence of EPR parameters for the broad *z1* line: (a) amplitude, *g*-factor and linewidth; (b) integrated intensity, the reciprocal of integrated intensity and the product of integrated intensity and temperature.

crystallographic sites with a strong crystal field (with $D > h\nu$) of predominantly axial symmetry with an appreciable rhombic distortion. These sites could be located at or near the surfaces of grains constituting the powder sample. The EPR integrated intensity *I* of these lines shows typical paramagnetic behaviour: it increases with a temperature decrease and $I^{-1}(T)$ changes linearly and intersects the temperature axis at T~0K (Fig. 6b).

In Fig. 7 the temperature dependence of EPR parameters for the broad *z1* line is presented. This is the most intense component at room temperature and a comparison with the other constituents shows that it contains 90% of the total spin concentration. Its temperature variation is very interesting – the line amplitude initially increases very weakly from RT with a temperature decrease, but about 70K it levels up and starts to decrease. Below 30K the line is too weak to calculate its EPR parameters reliably. The *g*-factor of this line reaches a minimum at ~60K and strongly increases with a temperature decrease while the linewidth increases until the line vanishes below 30K (Fig. 7a). The integrated intensity shows a pronounced peak at ~70 K (Fig. 7b). Such temperature behaviour of this line could be explained by postulating the existence of antiferromagnetic clusters consisting of Fe^{3+} spins. That system would be characterized by an energy gap of the order of 70K, whose contribution to the EPR spectrum would be wiped out below this temperature. A similar behaviour of the broad line was observed in $CrSbVO_6$, although the $I(T)$ function was peaked at a much lower temperature of 20K. Thus, the energy of the Fe^{3+} spin gap in $FeSbVO_6$ was

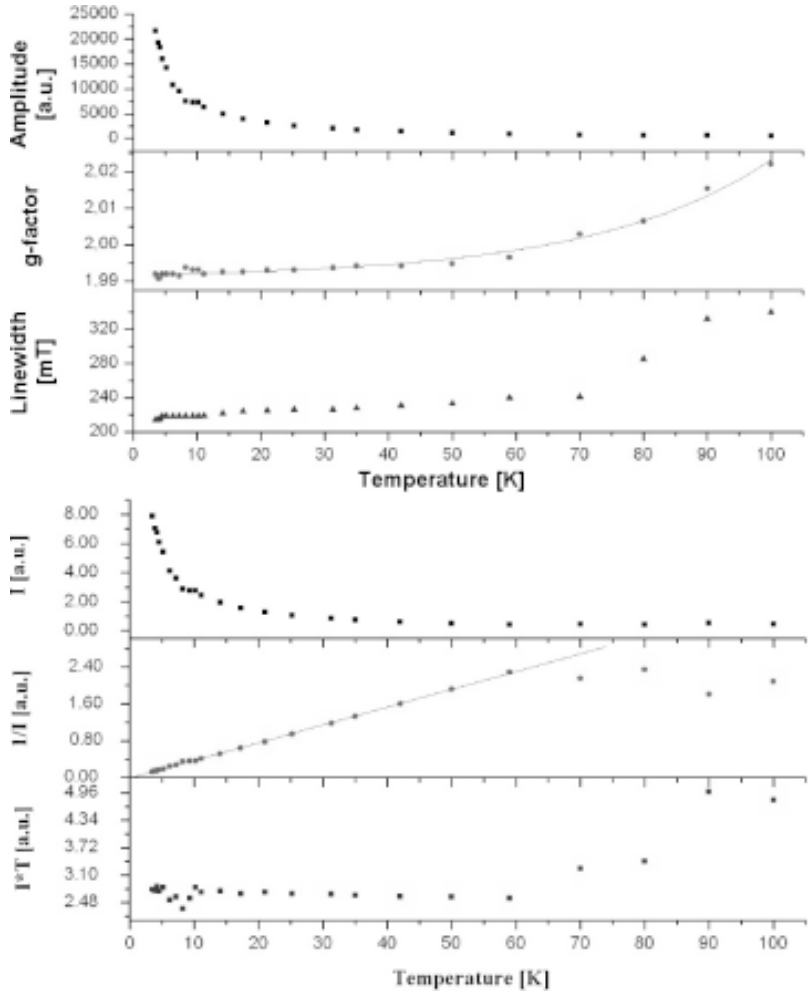

Fig. 8. Temperature dependence of EPR parameters for the *z2* line: (a) amplitude, *g*-factor and linewidth; (b) integrated intensity, the reciprocal of integrated intensity and the product of integrated intensity and temperature.

found to be much higher (three times) than the energy for the Cr^{3+} cluster in $CrSbVO_6$.

The other two components *z2* and *z3* show similar temperature behaviour. Fig. 8 shows the temperature dependence of EPR parameters for the *z2* line. The amplitude of both components increases and the linewidth decreases with a temperature decrease from RT. The *g*-factors of both lines are only weakly dependent on the temperature and significantly different being about ~2.0 and ~2.08 for the *z2* and *z3* lines, respectively. The temperature dependence of the integrated intensity of each components follows roughly the Curie-Weiss low, especially in the low temperature range (T<30K), with a small value of the Curie-Weiss temperature. It is assumed that these lines are produced by spin clusters, containing both V^{4+} and Fe^{3+} ions. Considering the placement of magnetic ions in the crystal structure of $FeSbVO_6$ (see Fig. 1) it is easy to notice that the probability of formation of spin clusters is very high. Regarding the measured values of *g*-factors it could be supposed that the cluster responsible for the *z2* component contains mostly V^{4+} ions while the cluster producing the *z3* component should be composed mainly from Fe^{3+} ions.

It would be interesting to compare the EPR results obtained on $FeSbVO_6$ with the previously studied $CrSbVO_6$ [18]. In Table 1 a comparison of the paramagnetic centres identified in both compounds is presented. The low-field lines observed in $FeSbVO_6$ at low temperatures and attributed to surface sites are absent in the $CrSbVO_6$ spectra. This does not necessarily mean that the Cr^{3+} ions avoid such low symmetry sites - a short relaxation time of such sites broadens the EPR lines and makes them unobservable. The narrow line, attributed to strongly coupled V^{4+} /VO^{2+} monomers in case of $FeSbVO_6$ shows striking differences in its tempera-

Table 1. Comparison of EPR centres in $FeSbVO_6$ and $CrSbVO_6$ [18].

EPR spectrum component		$FeSbVO_6$	$CrSbVO_6$
Low-field lines		Monomeric Fe^{3+} ions located at crystallographic sites with a strong crystal field (with $D>h\nu$) of predominantly axial symmetry with an appreciable rhombic distortion (at or near the surface)	Absent
Narrowline		Strongly coupled V^{4+}/VO^{2+} monomers	Strongly coupled V^{4+}/VO^{2+} and Cr^{3+} monomers
Broadline	*z1*	Antiferromagnetic clusters of Fe^{3+} spins	Antiferromagnetic V^{4+} dimers and spin clusters containing Cr^{3+} and V^{4+} ions
	z2	Spin clusters containing mostly V^{4+} ions	
	z3	Spin clusters containing mostly Fe^{3+} ions	

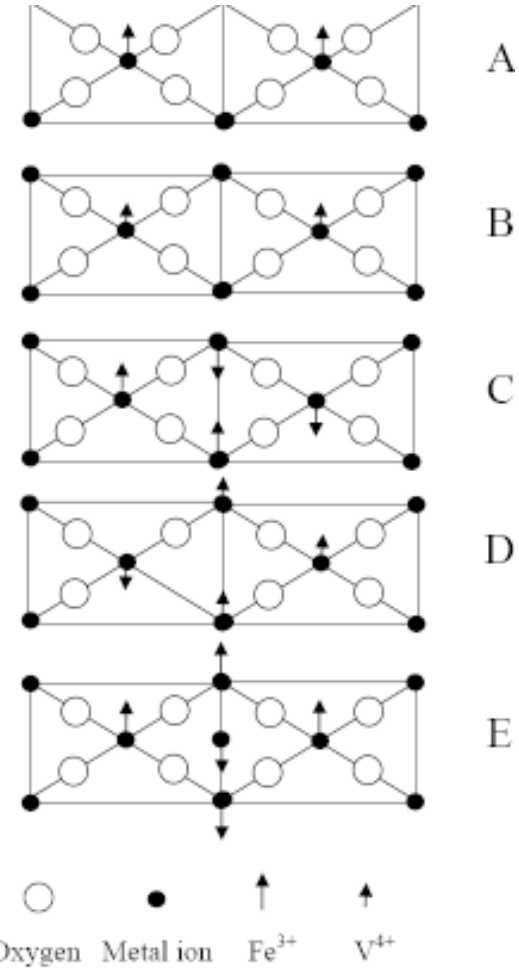

Fig. 9. Schematic representation of EPR paramagnetic centres in $FeSbVO_6$ accountable for: A – Fe^{3+} low-field line, B – narrow line, C – *z1* component of the broad line, D – *z2* component of the broad line, E – *z3* component of the broad line.

ture behaviour in both compounds. In $CrSbVO_6$, the temperature dependence of the linewidth and the integrated intensity of the narrow line are much more complicated than in $FeSbVO_6$, indicating a competition of magnetic interactions of at least two paramagnetic centres. The magnetic subsystem producing the narrow line in $FeSbVO_6$ seems to be more homogeneous and involves only vanadium species. In contrast, the broad line in $FeSbVO_6$ has to be deconvoluted on three lines indicating the contribution of ferromagnetic and antiferromagnetic spin dimers and clusters. A similar line in the EPR spectrum of $CrSbVO_6$ was described by only antiferromagnetic dimers and clusters (with a non-magnetic ground state). This might be a result of differences of the magnetic interaction between V^{4+} ions with Fe^{3+} and Cr^{3+} ions (the magnetic moment of free Fe^{3+} is 50% bigger than the magnetic moment of Cr^{3+}).

To speculate on the structure of the paramagnetic centres in $FeSbVO_6$ it would be advisable to examine the point defects in the rutile structure. In the rutile structure of $FeSbVO_6$, the oxygen atoms form octahedra, but only half of the octahedral sites are occupied by metal atoms. Thus, an unoccupied octahedral site could be chosen as the initial position for an interstitial defect which is located at the centre of the (010) or (100) faces. The following four intrinsic point defects in a rutile structure has been discussed at length in the literature: metal interstitial M_i, oxygen vacancy V_O, metal vacancy V_M, and oxygen interstitial O_i [25-28]. The metal interstitial M_i lies in an octahedral site similar to a lattice metal site, but the equatorial *M–O* bond length is much longer than the apical one. After relaxation, the clos-

est oxygen atoms, as well as the near metal atoms are pushed away, and the equatorial oxygen atoms are pulled towards M_i. For V_O vacancy, its three nearest neighbour metal atoms move outward and the nearest oxygen atoms move towards the vacancy. It should be noticed that the number of possible sites for the V_O vacancy is twice of that for the M_i vacancy, so the formation of V_O is more favoured than that of M_i. When metal vacancy V_M forms, the nearest metal atoms move to the vacancy, and the nearest oxygen atoms relax outward. In case of oxygen interstitial vacancy O_i, its nearest metal ions are attracted due to the fact that an oxygen atom occupies the centre of the octahedron while the oxygen ions are pushed away.

In Fig. 9 a very schematic representation of the paramagnetic centres responsible for all the observed EPR spectrum features in $FeSbVO_6$ has been shown. Two neighbouring unit cells of the $FeSbVO_6$ structure are presented with oxygen (large circle) and metal (small filled circle) ions. The magnetic moments of Fe^{3+} (long arrow) and V^{4+} (short arrow) are also drawn. As the low-field line is connected with Fe^{3+} ions at sites located at or near the surfaces of grains, the upper ions have been removed in (A). In (B), the monomeric V^{4+} ions are located in the neighbouring cells to allow for a rather strong magnetic interaction averaging out the hyperfine interaction and broadening the resonance line. In diagram (C), the Fe^{3+} ions are placed close to each other at metal lattice sites to form a cluster with an antiferromagnetic ground state. As the *z1* line produced by such cluster is most intense in the EPR spectrum of $FeSbVO_6$ it seems that the cluster does not involve any point defect discussed above. Diagrams (D) and (E) present schematically the centres generating lines *z2* and *z3*, respectively. As the intensity of those lines is much weaker it has been assumed that they are connected with point defects. Diagram D depicts the oxygen vacancy V_O defect involved into a vanadium cluster while diagram E presents the iron interstitial Fe_i defect that induces formation of the iron spin cluster.

Although the presence of the metal interstitial, oxygen vacancy, metal vacancy, and oxygen interstitial defects in the rutile structure is confirmed by literature data, the presence of these intrinsic defects, which leads to formation of magnetic centres in the $FeSbVO_6$ compound is by no means established and needs further confirmation by other techniques. Thus, the existence of clusters in the investigated samples of the $FeSbVO_6$ compound needs independent confirmation. Accordingly, the interpretation of the EPR results and the proposed models of paramagnetic centres and clusters should be taken as a working hypothesis awaiting verification by other magnetic methods.

4. CONCLUSIONS

An EPR study of magnetic properties of $FeSbVO_6$ in the 4-300K temperature range was carried out. At least four types of different paramagnetic centres were identified. At low temperatures and in low magnetic fields a complicated spectrum of isolated Fe^{3+} ions in a strong axial crystal field with a rhombic distortion was registered. A narrow EPR line arising from strongly interacting monomeric V^{4+}/VO^{2+} ions was observed in the whole investigated temperature range. An intense broad line was deconvoluted on three component lines attributed to the antiferromagnetic spin clusters of Fe^{3+} ions with a ~70K energy gap and other spin clusters containing Fe^{3+} and V^{4+} ions. The formation of spin clusters in $FeSbVO_6$ was promoted by a statistical distribution of magnetic ions and oxygen deficiency. A comparison of paramagnetic centres and interactions in $FeSbVO_6$ and $FeSbVO_6$ compounds was been made. The observed differences could be explained by different paramagnetic properties of the Fe^{3+} and Cr^{3+} ions and differences in their interaction with the V^{4+} ions.

REFERENCES

[1] S. Larrondo, B. Irigoyen, G. Baronetti and N. Amadeo // *Appl. Catal. A: General* **250** (2003) 279.

[2] V. P. Vislovskiy, N.T. Shamilov, A.M. Sardarly, V.Yu. Bychkov, M.Yu. Sinev, P. Ruiz, R. X. Valenzuela and V. Cort's Corber'an // *Chem. Eng. J.* **95** (2003) 37.

[3] D.W. Park, B. K. Park, D.K. Park and H.Ch. Woo // *Appl. Catal. A* **223** (2002) 215.

[4] N. Ballarini, F.Cavani, M. Cimini, F. Trifiro, R. Catani, U. Cornaro and D. Ghisletti // *Appl. Catal. A* **251** (2003) 49.

[5] N. Ballarini, F. Cavani, D. Ghisletti, R. Catani and U. Cornaro // *Catal Today* **78** (2003) 237.

[6] H.W. Zanthoff, W. Grünert, S. Buchholz, M. Heber, L. Stievano, F.E. Wagner and G.U. Wolf // *J. Mol. Catal. A: Chem.* **162** (2000) 443.

[7] A. Andersson, S. Hansen and A. Wickman // *Topics Catal.* **15** (2001) 103.

[8] M.O. Guerrero-Pérez, J.L.G. Fiero and M.A. Bańares // *Catal. Today* **78** (2003) 387.

[9] R. Irmawati, M.A. Razali, Y.H. Taufiq-Yap and Z. Zainal // *Catal. Today* **93–95** (2004) 631.

[10] J. Nilsson, A. Landa-Cánovas, S. Hansen and A. Andersson // *Catal. Today* **33** (1997) 97.
[11] G. Centi, S. Perathoner and F. Trifiro // *Appl. Catal. A* **157** (1997) 143.
[12] M.M. Bettahar, G. Costentin, L. Savary and J.C. Lavalley // *Appl. Catal. A* **145** (1996) 1.
[13] E.A. Mamedov and V. Cortes Corberan // *Appl. Catal. A* **127** (1995) 1.
[14] Y. Huang and P. Ruiz // *Appl. Surf. Sci.* **252** (2006) 7849.
[15] Z. Magagula and E. van Steen // *Catal. Today* **49** (1999) 155.
[16] E. Filipek and G. Dabrowska // *J. Mater. Sci.* **42** (2007) 4905.
[17] J. Isasi, M.L. Veiga, A. Jerez, M.L. López and C. Pico // *J. Mater. Chem.* **1** (1991) 1027.
[18] J. Typek, N. Guskos and E. Filipek // *J. Non-Cryst. Solids* **354** (2008) 4494.
[19] E. Filipek, G. Dabrowska and M. Piz, in press in *Alloys Comp*.
[20] J. Typek, E. Filipek, M. Maryniak and N. Guskos // *Materials Science-Poland* **23** (2005) 1047.
[21] B. Bleaney and K.W.H. Stevens // *Rep. Prog. Phys.* **16** (1953) 108.
[22] R.D. Dowsing and J.F. Gibson // *J. Chem. Phys.* **50** (1969) 294.
[23] K.S. Doctor, B.J. Gaffney, G. Alvarez and H.J. Silverstone // *J. Phys. Chem.* **97** (1993) 3028
[24] S. Gupta, N. Khanijo and A. Mansingh // *J. Non-Cryst. Solids* **181** (1995) 58.
[25] T.A. Egerton, E. Harris, E.J. Lawson, B. Mile and Ch.C. Rowlands // *Phys. Chem. Chem. Phys.* **3** (2001) 497.
[26] H. Peng // *Physics Letters A* **372** (2008) 1527.
[27] P.I. Kingsury, W.D.Ohlsen and O.W. Johnson // *Phys. Rev.* **175** (1968) 1091.
[28] G.-J. Shen and L.A. Bursil // *Proc. R. Soc. Lond. A* **405** (1986) 275.